UDE-Based Variable Impedance Control of Uncertain Robot Systems

Yiting Dong, *Student Member, IEEE*, and Beibei Ren, *Member, IEEE*

***Abstract*—A fundamental requirement in robot control is the capability to improve the robot–environment interaction performance. Motivated by the fact that humans are able to adapt limb impedance to stably interact with various environments with skillful dexterity, this paper investigates the variable impedance control for robots, subject to uncertainties from plant model or environment. The proposed variable impedance control assists the robot to perform given interaction tasks with its unknown environment and improves the overall robot–environment system performance. The stiffness, damping, and inertia can be changed during interaction tasks, which results in configuration-dependent impedance dynamics. The uncertainty and disturbance estimator (UDE) is used to approximate the plant model with only partial information known. The prominent feature of the UDE-based control is that only the bandwidth information of the unknown plant model is needed for the control design. A stability condition for selecting the stiffness, damping, and inertia in the impedance model is provided to guarantee the stability of the control system. Extensive simulation studies are carried out to illustrate the effectiveness of the proposed method.**

***Index Terms*—Impedance control, nonlinear systems, robot control, robot–environment interaction, uncertainty and disturbance estimator (UDE).**

I. Introduction

IN RECENT years, the control design of uncertain robot systems has received significant attention from both engineers and scientists interested in intelligent behaviors and skillful dexterity [1]–[4]. Impedance control is proposed as a control strategy for the realization of intelligent behavior and improving the interaction between a robot and its environment in many situations [5], [6]. Recently, impedance control has been used to solve for quadruped robots in [7], finger-arm robots in [8], constrained robots in [9], and rehabilitation robots in [10] and [11], as well as the application in robot–environment interaction in [12]–[14], human–robot collaboration in [15]–[17] and gait rehabilitation in [18]. Although previous research has handled the issue of robot–environment interaction, most works are based on fixed impedance-controlled systems, i.e., the stiffness, damping, and inertia are constant matrices. However, in unpredictable environmental events, the adoption of fixed impedance control is not a suitable strategy to ensure the high quality of performance, which is not just about repeatability and accuracy, but also determines the ability of robots to adapt their behaviors dynamically. Since humans continuously control the force exerted on an object by adapting their stiffness, damping, and inertia, in a similar way the robot should also be able to change the stiffness, damping, and inertia of its mechanical structure while performing an interaction task, so that the robot can adapt its behavior dynamically. Variable impedance control not only regulates the dynamic relationship between robot movements and contact forces but also gives the flexibility to change these dynamics during interaction tasks in which fixed impedance control is prone to failure [19], [20].

Recently, several works have studied the problem of the specification of variable impedance. In [21], Cartesian impedance control is proposed for rigid robots, where the direct feedback of contact force exerted by the environment can be avoided if the inertia shaping is not considered. Some research results have been developed based on the analysis in [21]. A passivity-based impedance control algorithm that allows to reproduce a time-varying stiffness is proposed in [22]. Variable impedance control of a redundant robotic manipulator executing a cooperative task with a human is proposed in [23], where the performance of human–robot interaction is enhanced by combined techniques of Cartesian impedance control and redundancy resolution. Indeed, Cartesian impedance control approach can avoid the effect of the external force. But in general, this kind of impedance is only suitable for applications where the velocity is low, and should be based on the assumption that the information of robot dynamics is known. Moreover, those control approaches in [21]–[23] bring about the problem of designing the damping matrix in an appropriate way.

As a matter of fact, force feedback is still required if the inertia reshaping is desired. If the natural inertia is preserved, a configuration-dependent damping matrix should be adopted to guarantee the stability of the whole system, which results in configuration-dependent impedance dynamics [24]. In [25], a variable impedance control approach depending on the contact force is proposed for robotic manipulators, where both stiffness and damping can be changed during the tasks, and a stability constraint that is related to the stiffness, and the time derivative of the stiffness and

Manuscript received August 15, 2017; accepted October 12, 2017. Date of publication November 20, 2017; date of current version November 19, 2019. This paper was recommended by Associate Editor R. Roberts. *(Corresponding author: Beibei Ren.)*

The authors are with the Department of Mechanical Engineering, Texas Tech University, Lubbock, TX 79409-1021 USA (e-mail: yiting.dong@ttu.edu; beibei.ren@ttu.edu).

Color versions of one or more of the figures in this paper are available online at http://ieeexplore.ieee.org.

Digital Object Identifier 10.1109/TSMC.2017.2767566

damping is studied. However, variable impedance control [25] is based on the assumption that the inertia remains constant, and the information of robot dynamics is known. Therefore, the problem of variable impedance control needs to be further investigated.

Recently, the control problem of unknown systems has gained much attention [26]–[30]. For control of uncertain robot systems, several strategies have been proposed to compensate the uncertainty. In [31], a backstepping approach is used to design a stable trajectory tracking controller for flexible-joint robotic manipulators, where an adaptive controller can compensate for parametric uncertainty and unknown bounded disturbances. Based on the backstepping approach, an adaptive dynamic surface controller is proposed with state feedback in [32] and output feedback in [33], where self-recurrent wavelet neural networks are used to observe the model uncertainty. Although previous research results have handled the issue of robot systems with uncertainty, those works either need the linear parametrization as prior knowledge in [31], or require the bounds information of NN approximate errors in [32] and [33]. In this paper, the uncertainty and disturbance estimator (UDE)-based variable impedance control is proposed for an uncertain robot, where the UDE technology does not need the linear parametrization or the bounds information of NN approximate errors. Motivated by the spirit of proposing an alternative control strategy to obtain a similar performance to time delay control in frequency domain, Zhong and Rees introduced the UDE control algorithm in [34], which is based on the assumption that a continuous signal can be estimated by using a filter with its appropriate bandwidth, to estimate the combined influence of disturbance and uncertainty. Since then, a number of UDE research results have been developed, such as for single-input single-output systems in [35], non-affine nonlinear systems in [36], uncertain linear time-invariant systems in [37], and sliding mode control in [38] and [39], as well as its wide applications to power flow control in [40], vertical take-off and landing aircraft in [41], wind turbine systems in [42], and piezoelectric stages in [43]. The significant feature of the UDE-based control is that it does not require any information about the uncertainty, except for its bandwidth. Moreover, this approach has a simple structure and is easy for the implementation and parameter tuning while bringing a good robust performance. Although the UDE-based control was applied to robotic control in [44], the results are only applicable in free space without environment interaction.

To address the above unsolved problem, in this paper, we consider an uncertain robot interacted with its unknown environment. The variable impedance control is developed for robot–environment interaction, and the UDE technology is used to approximate the unknown plant model of the robot. This paper is well motivated by the interaction control problem between an uncertain robot and its unknown environment. Compared to the existing work, the main contributions are highlighted as follows.

1) With respect to the classical impedance control, in this paper, new variable impedance control is developed for uncertain robot systems to improve the robot–environment interaction. The stiffness, damping, and inertia can be changed during the tasks, resulting in configuration-dependent impedance dynamics.
2) A stability condition for selecting the stiffness, damping, and inertia is provided to guarantee the stability of the whole system. The most important practical advantage of this stability condition is that it can be verified offline before executing interaction tasks.
3) The robot dynamics is not necessarily known in the proposed scheme by constructing a designed filter to estimate these unknown plant models online. And only the bandwidth of system model is required for the filter design. Furthermore, the proposed control has a simple system structure and is easy to be implemented and tuned while bringing a good robust performance.
4) Output feedback UDE-based control for robot systems is proposed due to the fact that some state information may not be measurable. The challenging problem of designing an output feedback controller using UDE is converted into the design of a low-pass filter.

The rest of this paper is structured as follows. Section II formulates the problem and contains a presentation of the impedance control. In Section III, variable impedance control based on the uncertainty and disturbance estimator is constructed for uncertain robots, and the stability of the whole system is established. Section IV shows the validation of the proposed strategy by simulation studies. Section V concludes this paper.

II. Problem Formulation and Preliminaries

A. System Description

In this paper, we investigate a typical robot–environment interaction system, which includes a robot with its unknown compliant environment, where force sensors are installed on the robot to measure the force exerted by the environment to the robot. According to the force detected by sensors, the whole system generates appropriate control input that derives the robot to a desired destination. Both the environment and robot dynamics are unknown.

Consider the following robotic dynamics in joint space [45]:

$$M(q)\ddot{q} + C(q,\dot{q})\dot{q} + G(q) = \tau + J^T(q)f \tag{1}$$

where $q,\ \dot{q},\ \ddot{q} \in \mathbb{R}^n$ are the position, velocity, and acceleration vectors in joint space, respectively; $M(q) \in \mathbb{R}^{n\times n}$, $C(q,\dot{q})\dot{q} \in \mathbb{R}^n$, and $G(q) \in \mathbb{R}^n$ are symmetric bounded positive-definite inertia matrix, Coriolis and Centrifugal force, and gravitational force, respectively; $\tau \in \mathbb{R}^n$ is the vector of control input; $J(q) \in \mathbb{R}^{n\times n}$ is the Jacobian matrix; and $f \in \mathbb{R}^n$ is the force exerted by the compliant environment. In the robot–environment interaction task studied in this paper, $M(q)$, $C(q,\dot{q})$, and $G(q)$ cannot be obtained beforehand.

Let $x,\ \dot{x},\ \ddot{x} \in \mathbb{R}^n$ are the position, velocity, and acceleration vectors of the end-effector in Cartesian space, respectively. Given that the interaction is described in Cartesian space, by using the transformation between joint space and Cartesian space: $\dot{x} = J(q)\dot{q}$, the Cartesian robotic dynamics is considered as [45]

$$M_x(q)\ddot{x} + C_x(q,\dot{q})\dot{x} + G_x(q) = F + f \tag{2}$$

where $M_x(q) = J^{-T}(q)M(q)J^{-1}(q)$, $C_x(q,\dot{q}) = J^{-T}(q)(C(q,\dot{q}) - M(q)J^{-1}(q)\dot{J}(q))J^{-1}(q)$, $G_x(q) = J^{-T}(q)G(q)$ and $F = J^{-T}(q)\tau$.

Property 1 [46]: Matrix $M_x(q)$ is symmetric and positive definite.

Property 2 [46]: Matrix $\dot{M}_x(q) - 2C_x(q,\dot{q})$ is a skew-symmetric matrix, i.e., $\epsilon^T\big(\dot{M}_x(q) - 2C_x(q,\dot{q})\big)\epsilon = 0$, $\forall \epsilon \in \mathbb{R}^n$.

Assumption 1 [5], [45]: The compliant environment may behave as a simple mechanical system undergoing small but finite deformation in response to an applied force when contact occurs.

B. Problem Statement

The objective of impedance control is to satisfy the following impedance model between x and f:

$$M_d(\ddot{x} - \ddot{x}_d) + C_d(\dot{x} - \dot{x}_d) + K_d(x - x_d) = f \tag{3}$$

where $x_d \in \mathbb{R}^n$ is a reference trajectory for the end-effector, M_d, C_d, $K_d \in \mathbb{R}^{n\times n}$ are the desired inertia, damping, and stiffness matrices, respectively. In general, the matrices M_d, C_d, and K_d are specified by the user so that the dynamics in (3) possesses the desired characteristics [45]. For example, the stiffness describes the property of a robot to resist deformation, which is sometimes referred to as rigidity. In particular, high stiffness results in the fact that the robot rigidity is high and the robot uses a large force to reach a given position. The contact force f can be measured by sensors.

Note that there are two phases during the robot–environment interaction, i.e., contact phase and noncontact phase. In noncontact phase, there are $f = 0$, and $x = x_d$, $\forall t > 0$ (if $x(0) = x_d(0)$), which corresponds to trajectory tracking in the absence of environmental contact. In contact phase, the actual position x will be redefined according to the interaction force f, inertia M_d, damping C_d, and stiffness K_d. If these matrices are constant symmetric positive definite, the system will be asymptotically stable [25].

In this paper, we are concerned with variable impedance control, where the desired impedance model is given by

$$M_d(t)(\ddot{x} - \ddot{x}_d) + C_d(t)(\dot{x} - \dot{x}_d) + K_d(t)(x - x_d) = f \tag{4}$$

where $M_d(t)$, $C_d(t)$, and $K_d(t)$ are time-varying matrices. Our goal is to modify the conventional impedance control in order to allow time-varying inertia, damping, and stiffness while preserving a stable interactive behavior in Cartesian space.

Definition 1 [47]: A dynamical system $\sum$ with supply rate $w(t)$ is said to be dissipative if there exists a non-negative function $S : \mathbb{X} \to \mathbb{R}^+$, called the storage function, such that for all $t \in (t_0, t_1)$

$$S(x_0) + \int_{t_0}^{t_1} w(t)dt \geq S(x_1) \tag{5}$$

where $x_0 \in \mathbb{X}$ and $x_1 \in \mathbb{X}$. The above inequality is called the dissipation inequality.

III. Control Design

The objective of variable impedance control can be achieved if the dynamical system (2) satisfies the target impedance model (4). From (2), there is

$$\ddot{x} = M_x^{-1}(q)\big[F + f - C_x(q,\dot{q})\dot{x} - G_x(q)\big]. \tag{6}$$

To facilitate the subsequent control design, it is assumed that the unknown matrix $M_x(q)$ can be separated as a user-defined nonsingular constant diagonal matrix denoted by M_{xo} and an uncertain part represented by $\Delta M_x(q) = M_x(q) - M_{xo}$. Substituting $\Delta M_x(q) = M_x(q) - M_{xo}$ to (6), the robotic dynamics can be re-expressed as

$$\ddot{x} = M_{xo}^{-1}F + \Delta M_x^{-1}(q)F + M_x^{-1}(q)\big[f - C_x(q,\dot{q})\dot{x} - G_x(q)\big]. \tag{7}$$

The generalized tracking error e, and its first derivative $\dot{e}$ are defined as follows:

$$e = x - x_d, \quad \dot{e} = \dot{x} - \dot{x}_d. \tag{8}$$

Substituting (8) to (4), the desired error dynamics can be obtained as

$$M_d(t)(\ddot{x} - \ddot{x}_d) + C_d(t)\dot{e} + K_d(t)e = f. \tag{9}$$

Substituting (7) to (9), there is

$$\begin{aligned} M_d(t)\Big\{&M_{xo}^{-1}F + \Delta M_x^{-1}(q)F + M_x^{-1}(q) \\ &\times \big[f - C_x(q,\dot{q})\dot{x} - G_x(q)\big] - \ddot{x}_d\Big\} \\ &+ C_d(t)\dot{e} + K_d(t)e = f. \end{aligned} \tag{10}$$

Based on (10), the control signal F should satisfy

$$M_d(t)M_{xo}^{-1}F = f - u_d + M_d(t)\ddot{x}_d - C_d(t)\dot{e} - K_d(t)e \tag{11}$$

where

$$u_d = M_d(t)\Big\{\Delta M_x^{-1}(q)F + M_x^{-1}(q)\big[f - C_x(q,\dot{q})\dot{x} - G_x(q)\big]\Big\} \tag{12}$$

represents the lumped uncertainty term in (10), including the unknown terms $M_x(q)$, $C_x(q,\dot{q})$, $G_x(q)$, and $\Delta M_x(q)$. According to (7), u_d can be denoted as

$$u_d = M_d(t)\Big(\ddot{x} - M_{xo}^{-1}F\Big) \tag{13}$$

which illustrates that the uncertainty u_d can be obtained from the known dynamics of system and control signal. However, it cannot be directly used to formulate a control law. Assume that the frequency range of a signal is limited, the signal can be estimated using a filter with the appropriate bandwidth information, then the procedure of UDE-based control design given in [34] is adopted to handle the uncertainty so that a control law is derived. Assume that $G_f(s)$ is a strictly proper stable filter with the unity gain and zero phase shift over the spectrum of u_d and zero gain elsewhere. Then, u_d can be approximated by

$$\hat{u}_d = \mathcal{L}^{-1}\{G_f(s)\} * \Big[M_d(t)\Big(\ddot{x} - M_{xo}^{-1}F\Big)\Big] \tag{14}$$

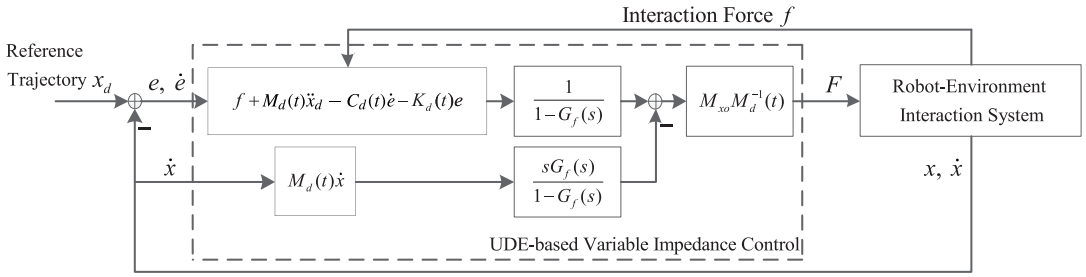

Fig. 1. Proposed UDE-based variable impedance control strategy.

where $\hat{u}_d$ is an estimate of u_d, "$*$" denotes the convolution operation, and $\mathcal{L}^{-1}\{\cdot\}$ is the inverse Laplace transform operator. Replacing u_d with $\hat{u}_d$ in (11), there is

$$M_d(t)M_{xo}^{-1}F = f + M_d(t)\ddot{x}_d - C_d(t)\dot{e} - K_d(t)e - \mathcal{L}^{-1}\{G_f(s)\} * \left[M_d(t)\left(\ddot{x} - M_{xo}^{-1}F\right)\right]. \quad (15)$$

Furthermore, the UDE-based variable impedance control can be derived from (15) as

$$F = M_{xo}M_d^{-1}(t)\left\{\mathcal{L}^{-1}\left\{\frac{1}{1-G_f(s)}\right\} * \left[f + M_d(t)\ddot{x}_d - C_d(t)\dot{e} - K_d(t)e\right] - \mathcal{L}^{-1}\left\{\frac{sG_f(s)}{1-G_f(s)}\right\} * [M_d(t)\dot{x}]\right\}. \quad (16)$$

Fig. 1 depicts the proposed control strategy. According to the tracking error and the interaction force detected by force sensors, the UDE-based variable impedance control can generate an appropriate control signal which can drive the uncertain robot to a desired destination.

Remark 1: The proposed control (16) requires full states, x and $\dot{x}$, to be implemented. However, some state information may not be measurable due to practical issues such as in the absence of velocity sensors. Thus, an output feedback control scheme can be derived from (16) as

$$F = M_{xo}M_d^{-1}(t)\left\{\mathcal{L}^{-1}\left\{\frac{1}{1-G_f(s)}\right\} * \left[f + M_d(t)\ddot{x}_d - K_d(t)e\right] - \mathcal{L}^{-1}\left\{\frac{s}{1-G_f(s)}\right\} * C_d(t)e - \mathcal{L}^{-1}\left\{\frac{s^2G_f(s)}{1-G_f(s)}\right\} * [M_d(t)x]\right\}. \quad (17)$$

Clearly, the relative degree of the filter $G_f(s)$ in (17) should be no less than 2 to make sure that the control structure is realizable, i.e., $([s^2G_f(s)]/[1-G_f(s)])$ should be proper. Equation (17) implies that the challenging problem of designing an output feedback controller is converted into the design of a low-pass filter.

Remark 2 [21]: In the desired impedance model (4), the desired inertia matrix $M_d(t)$ can be designed in principle such that its eigenvectors coincide with the eigenvectors of $K_d(t)$. The design of $C_d(t)$ should take into account the particular structure and the change of $M_d(t)$ during movement.

Theorem 1: Consider the closed-loop system consisting of the robotic dynamics described by (2) and the UDE-based control (16). Assume that the filter $G_f(s)$ in (16) is chosen appropriately as a strictly proper stable filter with unity gain and zero phase shift over the spectrum of the uncertainty u_d and zero gain elsewhere. Then for any bounded initial conditions, let the inertia $M_d(t)$, damping $D_d(t)$ and stiffness $K_d(t)$ be symmetric, positive definite, and continuously differentiable time-varying matrices, there always exists a nominal part $C_o(t)$ such that, $\dot{M}_d(t) - 2C_o(t)$ is skew symmetric. It can be concluded that the desired impedance model (4) is achieved, and all signals in the closed-loop system are bounded, if there exists a constant $\alpha > 0$, such that $\forall t \geq 0$:

1) $C_d(t) - \alpha M_d(t) - C_o(t)$ is positive semi-definite;
2) $\alpha K_d(t) - (1/2)\dot{K}_d(t) - (1/2)\alpha\dot{C}_d(t) + \alpha\dot{C}_o(t)$ is positive semi-definite.

Proof: Consider the Lyapunov function candidate as

$$V(t) = \frac{1}{2}(\dot{e} + \alpha e)^T M_d(t)(\dot{e} + \alpha e) + \frac{1}{2}e^T\beta(t)e \quad (18)$$

where

$$\beta(t) = K_d(t) + \alpha C_d(t) - \alpha^2 M_d(t) - 2\alpha C_o(t) \quad (19)$$

with a positive constant α chosen, $\beta(t)$ is positive definite for all $t > 0$, which implies that $V(t)$ is also positive definite. Differentiating (18) with respect to time yields

$$\dot{V}(t) = (\dot{e} + \alpha e)^T M_d(t)(\ddot{e} + \alpha\dot{e}) + \frac{1}{2}(\dot{e} + \alpha e)^T\dot{M}_d(t)(\dot{e} + \alpha e) + e^T\beta(t)\dot{e} + \frac{1}{2}e^T\dot{\beta}(t)e. \quad (20)$$

Substituting the desired impedance model (4) to (20) yields

$$\dot{V}(t) = (\dot{e} + \alpha e)^T(f - C_d(t)\dot{e} - K_d(t)e) + (\dot{e} + \alpha e)^T M_d(t)\alpha\dot{e} + \frac{1}{2}(\dot{e} + \alpha e)^T\dot{M}_d(t)(\dot{e} + \alpha e) + e^T\beta(t)\dot{e} + \frac{1}{2}e^T\dot{\beta}(t)e. \quad (21)$$

For any $M_d(t)$, there always exists a nominal part $C_o(t)$ such that $\dot{M}_d(t) - 2C_o(t)$ is skew symmetric, i.e., $(\dot{e}+\alpha e)^T(\dot{M}_d(t) - 2C_o(t))(\dot{e} + \alpha e) = 0$. Then, in order to eliminate the term $(1/2)(\dot{e}+\alpha e)^T\dot{M}_d(t)(\dot{e}+\alpha e)$, subtracting $(\dot{e}+\alpha e)^T C_o(t)(\dot{e}+\alpha e)$ from both sides of (21) leads to

$$\dot{V}(t) = (\dot{e} + \alpha e)^T f - \dot{e}^T(C_d(t) - \alpha M_d(t) - C_o(t))\dot{e} - \dot{e}^T\left(K_d(t) + \alpha C_d(t) - \alpha^2 M_d(t) - 2\alpha C_o(t)\right)e - e^T\left(\alpha K_d(t) - \alpha^2 C_o(t)\right)e + e^T\beta(t)\dot{e} + \frac{1}{2}e^T\dot{\beta}(t)e. \quad (22)$$

The time derivative of (19) is calculated as

$$\dot{\beta}(t) = \dot{K}_d(t) + \alpha\dot{C}_d(t) - \alpha^2\dot{M}_d(t) - 2\alpha\dot{C}_o(t). \tag{23}$$

In order to eliminate the cross term between e and $\dot{e}$ in (22), substituting (19) and (23) to (22), there is

$$\dot{V}(t) = (\dot{e} + \alpha e)^T f - \dot{e}^T(C_d(t) - \alpha M_d(t) - C_o(t))\dot{e} - e^T\left(\alpha K_d(t) - \frac{1}{2}\dot{K}_d(t) - \frac{1}{2}\alpha\dot{C}_d(t) + \alpha\dot{C}_o(t)\right)e. \tag{24}$$

Next, the stability of the closed-loop system will be discussed in two phases, i.e., noncontact phase and contact phase.

1) When in noncontact phase, there is $f = 0$. Then, substituting $f = 0$ to (24), results in

$$\dot{V}(t) = -\dot{e}^T(C_d(t) - \alpha M_d(t) - C_o(t))\dot{e} - e^T\left(\alpha K_d(t) - \frac{1}{2}\dot{K}_d(t) - \frac{1}{2}\alpha\dot{C}_d(t) + \alpha\dot{C}_o(t)\right)e. \tag{25}$$

If there exist $\alpha > 0$ and $C_o(t) > 0$ satisfying both $C_d(t) - \alpha M_d(t) - C_o(t)$ and $\alpha K_d(t) - (1/2)\dot{K}_d(t) - (1/2)\alpha\dot{C}_d(t) + \alpha\dot{C}_o(t)$ are positive semi-definite in noncontact phase, it can be concluded that $\dot{V}(t) \leq 0$, and the system (2) is uniformly stable in noncontact phase.

2) When in contact phase, i.e., $f \neq 0$, if there also exist $\alpha > 0$ and $C_o(t) > 0$ satisfying both $C_d(t) - \alpha M_d(t) - C_o(t)$ and $\alpha K_d(t) - (1/2)\dot{K}_d(t) - (1/2)\alpha\dot{C}_d(t) + \alpha\dot{C}_o(t)$ are positive semi-definite, there is

$$\dot{V}(t) \leq (\dot{e} + \alpha e)^T f \tag{26}$$

which implies the following dissipation inequality according to Definition 1:

$$V(t) \leq V(0) + \int_0^t (\dot{e} + \alpha e)^T f d\tau. \tag{27}$$

Dissipation ensures a stable behavior of the system in contact phase.

Therefore, it can be concluded that the closed-loop system is stable if there exists $\alpha > 0$ satisfying both $C_d(t) - \alpha M_d(t) - C_o(t)$ and $\alpha K_d(t) - (1/2)\dot{K}_d(t) - (1/2)\alpha\dot{C}_d(t) + \alpha\dot{C}_o(t)$ are positive semi-definite. This completes the proof. ■

Remark 3: The theoretical principle of the filter selection is that, the filter $G_f(s)$ should be designed with the unity gain and zero phase shift over the spectrum of u_d and zero gain elsewhere [34]. The detailed guideline of the filter selection is provided in [37] and [48]. However, in practice, due to the hardware limitations, the filter parameter cannot be chosen too small. Also, the filter with too wide bandwidth will introduce sensor noise with high frequency, and thus might degrade the performance of the UDE-based controller. Therefore, how to select the filter depends on the specific application including the hardware capability and the performance requirements.

IV. Extensive Simulation Studies

To demonstrate the effectiveness of the proposed variable impedance control, simulation studies are carried out using a robot–environment interaction system shown in Fig. 2 for an imitation of wiping tasks. Fig. 2(a) shows a 2-link robotic manipulator with a rigid end-effector, which is interacted with a wall. The schematic diagram of this system is shown in Fig. 2(b), where the wall is located on the path of the robot motion. Variable impedance control is introduced to tackle the interaction between the robot and the wall, so that the robot should follow the reference position trajectory x_d in noncontact phase while the desired destination is regulated according to the force exerted by the wall during contact phase.

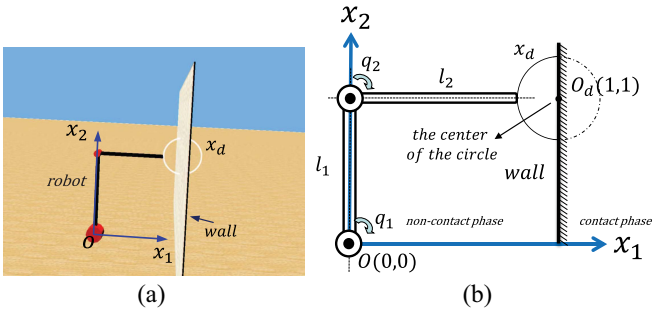

Fig. 2. Simulation scenario. (a) Robot–environment interaction system. (b) Schematic diagram.

TABLE I
Robot Parameters Modified From [49]

Parameter	Description	Value
m_1	Mass of link 1	2.00 kg
m_2	Mass of link 2	0.85 kg
l_1	Length of link 1	1.00 m
l_2	Length of link 2	0.80 m
I_1	Inertia of link 1	0.500 kgm^2
I_2	Inertia of link 2	0.136 kgm^2

A. Simulation Platform

Fig. 2 shows the robotic dynamics in Cartesian space (2) with system parameters given in Table I, which are modified from [49]. Let $x = [x_1, x_2]^T$, $e = [e_1, e_2]^T$, $f = [f_1, f_2]^T$ and $F = [F_1, F_2]^T$. The initial position and velocity of the robot are given as $x(0) = [0.80\ 1.00]^T$ and $\dot{x}(0) = [0\ 0]^T$. The initial vectors in joint space are set as $q(0) = [(\pi/2)\ (\pi/2)]^T$ and $\dot{q}(0) = [0\ 0]^T$. The reference trajectory is described by

$$x_d(t) = \begin{bmatrix} x_{d1}(t) \\ x_{d2}(t) \end{bmatrix} = \begin{bmatrix} 1.0 - 0.2\cos(\frac{1}{2}\pi t) \\ 1.0 + 0.2\sin(\frac{1}{2}\pi t) \end{bmatrix} \tag{28}$$

which is a circle shown in Fig. 2(b), with center O_d. Another parameter is set as: $M_{xo} = \text{diag}[0.15]$.

B. Comparison to Fixed Impedance Control

In this section, the comparison to a fixed impedance controller is carried out to illustrate the effectiveness of the proposed variable impedance controller. The reference trajectory is given by (28). Theorem 1 guarantees the closed-system is stable if a filter $G_f(s)$ is chosen appropriately as a strictly proper stable filter with unity gain and zero phase shift over the spectrum of the uncertainty u_d and zero gain elsewhere. In this case, it is sufficient to choose $G_f(s)$ as a first-order low-pass filter $G_f(s) = [1/(Ts + 1)]$ where T is chosen as a small enough positive number to ensure that the bandwidth of

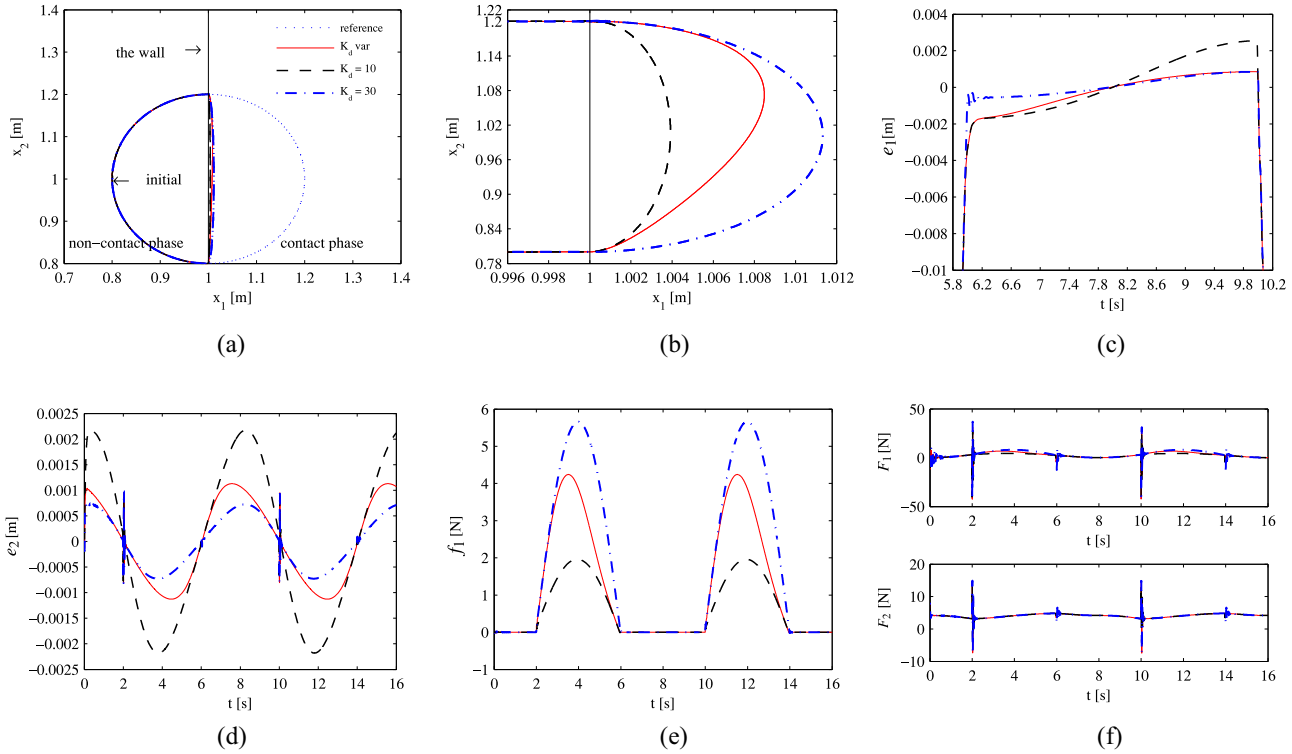

Fig. 3. Simulation results for case B1: comparison with the proposed scheme (16) with variable stiffness, low constant stiffness $K_d = 10$ and high constant stiffness $K_d = 30$. (a) Positions in Cartesian space. (b) Zoomed-in view positions in contact phase. (c) Zoomed-in view tracking error e_1 in noncontact phase. (d) Zoomed-in view tracking error e_2 in noncontact phase. (e) External force. (f) Control inputs.

$G_f(s)$ covers the spectrum of u_d. The first-order low-pass filter is chosen with $T = 0.01$ s. Based on Remark 2, the desired inertia, damping and stiffness are given by

$$M_d(t) = \text{diag}\left[0.0005 \sin\left(\frac{1}{2}\pi t\right) + 0.001\right] \tag{29}$$

$$C_d(t) = \text{diag}\left[0.5 \sin\left(\frac{1}{2}\pi t\right) + 1\right] \tag{30}$$

$$K_d(t) = \text{diag}\left[10 \sin\left(\frac{1}{2}\pi t\right) + 20\right]. \tag{31}$$

For the impedance parameters defined above, two cases are considered and tested.

Case B1: Comparison with the proposed scheme (16) with variable stiffness, low constant stiffness $K_d = 10$ and high constant stiffness $K_d = 30$.

The comparison simulation results are given in Fig. 3. The tracking performance in Cartesian space is shown in Fig. 3(a). From Fig. 3(a), it can be observed that the end-effector tracks the reference trajectory in noncontact phase. When the external force exerted by the wall is applied to the robot end-effector in contact phase, the desired destination is regulated and the end-effector slides along the wall. Fig. 3(b) gives the zoomed-in view performance in contact phase. It is clear that the wall undergoes small but finite deformation when contact occurs. It is also remarkable that the performance in the case of variable stiffness reaches intermediate values with respect to those in the case of low and high constant stiffness. In addition, Fig. 3(c) and (d) plots the tracking errors in noncontact phase.

It is worth noticing that, from Fig. 3(b), when constant low stiffness is used, the position of end-effector almost matches the desired one. However, from Fig. 3(c) and (d), when the robot moves in noncontact phase, the tracking error in the case of constant low stiffness is significant. Besides, although the deformation of the wall in the case of constant high stiffness is higher than that in the case of constant low stiffness, the tracking error goes to a small value near zero. It can be argued that, with respect to the interaction performance in contact phase and the tracking performance in noncontact phase, the use of variable stiffness allows to reach a good compromise compared to the cases of constant high and low stiffness.

Fig. 3(e) shows the external force, and the control inputs are plotted in Fig. 3(f). It is noted that there are a few oscillations while the robot comes in contact with the wall. This is due to the change of the unknown environment but the control force tends immediately to be smooth by using the proposed control.

Case B2: Comparison with the proposed scheme (16) with variable damping, low constant damping $C_d = 0.5$ and high constant damping $C_d = 1.5$.

The comparison results are given in Fig. 4. The tracking performance in Cartesian space is plotted in Fig. 4(a). In contact phase, it can be observed that the position of the end-effector in the case of variable damping does not change significantly compared with that in the case of constant low and high damping. Fig. 4(b) and (c) shows the zoomed-in view tracking errors in noncontact phase. It is clear that the tracking error in the case of variable damping reaches intermediate values with respect to those in the case of constant low and high damping. On the other hand, the zoomed-in view velocity is given in Fig. 4(d) and (e).

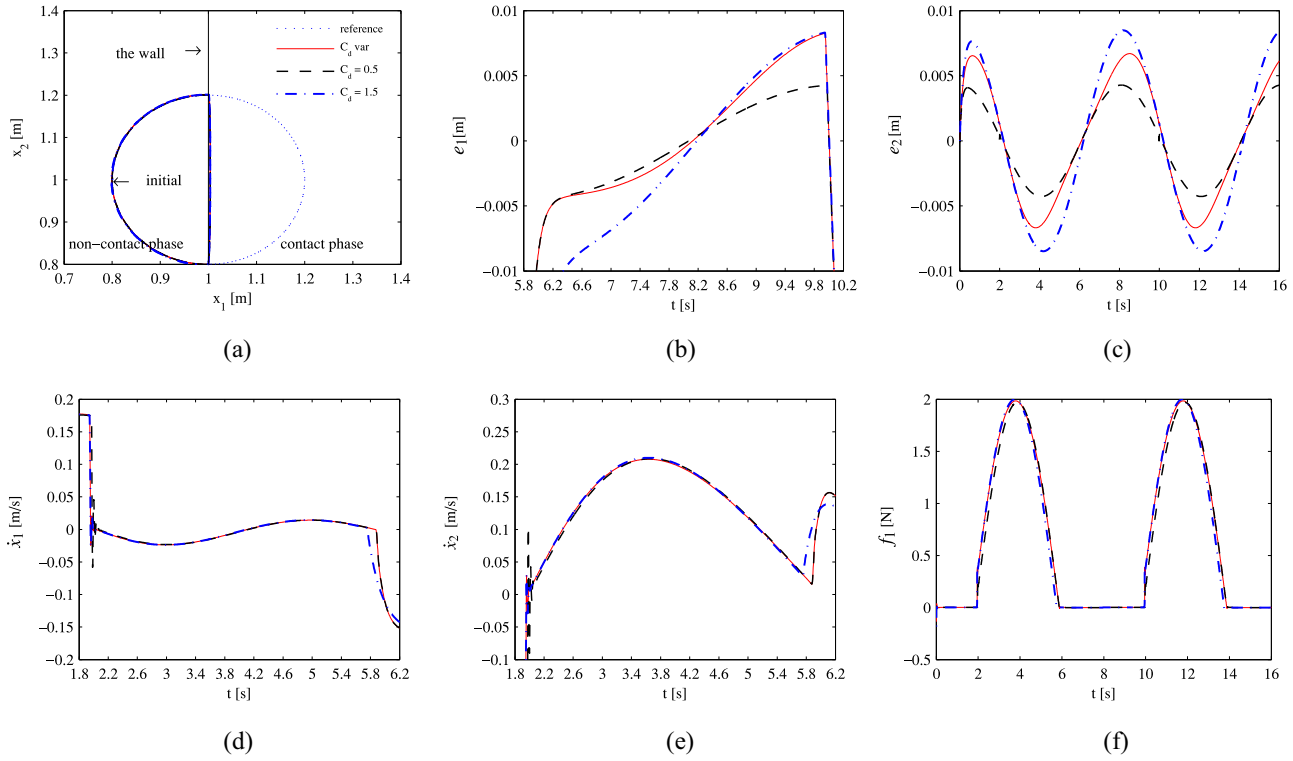

Fig. 4. Simulation results for case B2: comparison with the proposed scheme (16) with variable damping, low constant damping $C_d = 0.5$ and high constant damping $C_d = 1.5$. (a) Positions in Cartesian space. (b) Zoomed-in view tracking error e_1 in noncontact phase. (c) Zoomed-in view tracking error e_2 in noncontact phase. (d) Zoomed-in view velocity $\dot{x}_1$ in contact phase. (e) Zoomed-in view velocity $\dot{x}_2$ in contact phase. (f) External force.

It is noted that, from Fig. 4(b) and (c), when the low damping is applied, the tracking error in noncontact phase is small and the tracking performance almost matches the desired one. However, in terms of the velocity in contact phase, the overshoot in the case of low damping is remarkable (plotted in Fig. 4(d) and (e) when $t \in [1.8, 2.2]$). Although there exist some oscillations in other cases when $t \in [1.8, 2.2]$, the overshoots are smaller and the velocity converges to stable smoothly and quickly. It is concluded that, in terms of the tracking error in noncontact phase and the velocity profiles in contact phase, the use of variable damping tends to have a good compromise compared to the cases of constant low and high damping. Fig. 4(f) gives the external forces exerted by the wall.

In addition, the inertial behavior is not investigated in this paper where a slow interaction task is considered, as the inertial behavior declines and vanishes for slow movements [50] and it is not necessary in many applications [21].

C. Guidelines for Selecting Impedance Parameters

In this section, the guidelines for selecting impedance parameters in the impedance model (4) will be discussed. Although the stability of the closed-loop system is guaranteed, the interaction performance is mainly influenced by impedance parameters. Our idea is to change the magnitude or the frequency of the variable stiffness and variable damping in order to improve the performance in terms of accuracy, with other parameters being the same as those previously defined in Section IV-B. Different cases are considered.

Case C1 (Effect of the Magnitude of Stiffness): Consider constant inertia and damping, with different magnitudes of stiffness, i.e., $M_d(t) = 0.001$, $C_d(t) = 0.5$, $K_{d1}(t) = \text{diag}[2\sin([1/2]\pi t) + 5]$, $K_{d2}(t) = \text{diag}[2\sin([1/2]\pi t) + 10]$, and $K_{d3}(t) = \text{diag}[2\sin([1/2]\pi t) + 30]$. The simulation results for case C1 are plotted in Fig. 5. Fig. 5(a) shows the position of the end-effector in Cartesian space. The zoomed-in view performance in contact phase and the external force are given in Fig. 5(b) and (c), respectively. It can be observed that, when the magnitude of stiffness is increasing, both the deformation of the wall and the external force are increasing significantly. In addition, the zoomed-in view tracking error in noncontact phase is given in Fig. 5(d) and (e).

It is worth noticing that, the deformation of the wall is remarkably influenced by the magnitude of stiffness, because the decreasing magnitude of stiffness usually results in the decreasing of external force, which actually causes a low deformation of the wall. However, from Fig. 5(d) and (e), the tracking error in the case of low magnitude of stiffness reaches a large value. It shows that, how to choose the magnitude of stiffness $K_d(t)$ depends on the specific application including the performance requirements and the hardware capability. From Fig. 5(f), it can be seen that there are some oscillations in the control input. This is due to the change of the unknown environment but the control input tends to smooth immediately by using the proposed control.

Case C2 (Effect of the Frequency of Stiffness): Consider constant inertia and damping, with different frequencies of stiffness, i.e., $M_d(t) = 0.001$, $C_d(t) = 0.5$, $K_{d4}(t) = \text{diag}[2\sin([1/2]\pi t) + 10]$, $K_{d5}(t) = \text{diag}[2\sin(5\pi t) + 10]$ and

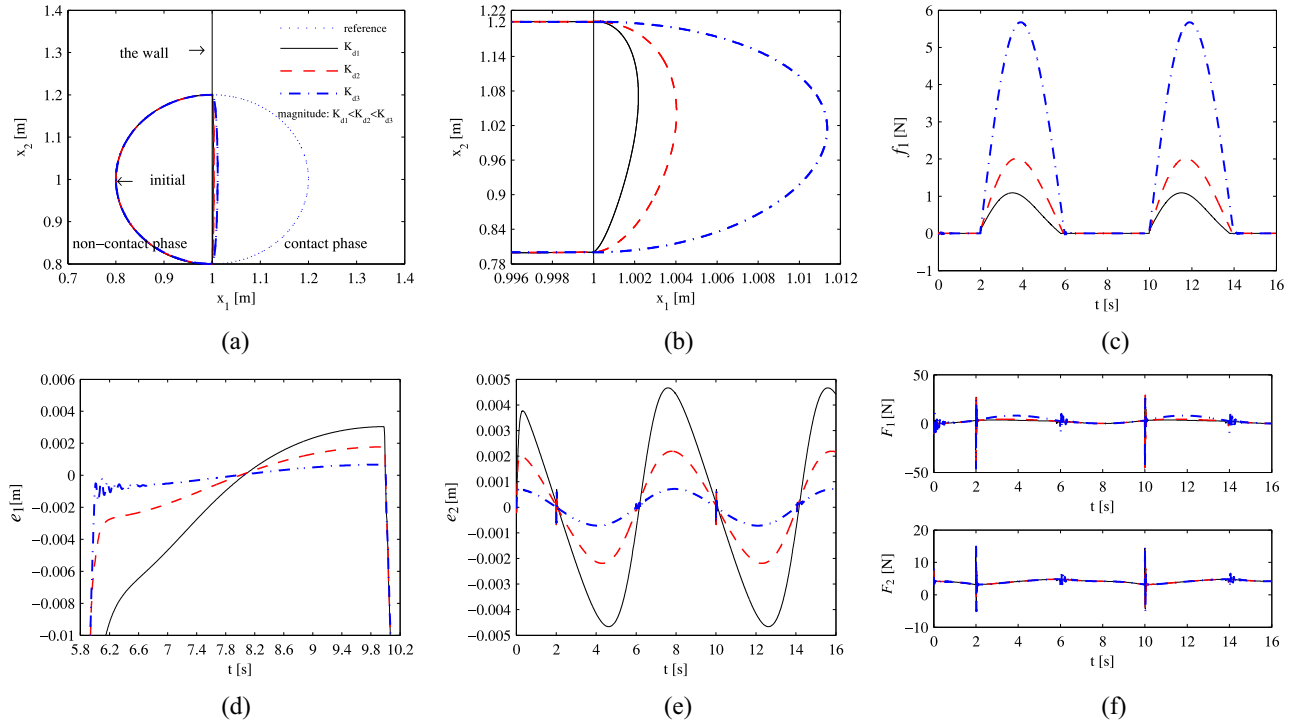

Fig. 5. Simulation results for case C1: constant inertia and damping, with different magnitudes of stiffness, i.e., $M_d(t) = 0.001$, $C_d(t) = 0.5$, $K_{d1}(t) = \text{diag}[2\sin([1/2]\pi t) + 5]$, $K_{d2}(t) = \text{diag}[2\sin([1/2]\pi t) + 10]$, and $K_{d3}(t) = \text{diag}[2\sin([1/2]\pi t) + 30]$. (a) Positions in Cartesian space. (b) Zoomed-in view positions in contact phase. (c) External force. (d) Zoomed-in view tracking error e_1 in noncontact phase. (e) Zoomed-in view tracking error e_2 in noncontact phase. (f) Control inputs.

$K_{d6}(t) = \text{diag}[2\sin(15\pi t) + 10]$. The simulation results with different frequencies of variable stiffness are given in Fig. 6. The position of the end-effector in Cartesian space is plotted in Fig. 6(a). The zoomed-in view interaction performance and the external force are given in Fig. 6(b) and (c), respectively. It is clear that, when the frequency of stiffness increases, both the interaction performance and the external force are oscillating apparently. In addition, the zoomed-in view tracking error in noncontact phase is given in Fig. 6(d) and (e), which also illustrates that the tracking error in the case of high frequency of stiffness is oscillating remarkably. It can be concluded that, $K_d(t)$ should have a low frequency in order to reduce the tracking errors and oscillations in practice. The control input is given in Fig. 6(f), and the oscillation of the control input results from the environmental change.

Case C3 (Effect of the Magnitude of Damping): Consider constant inertia and stiffness, with different magnitudes of damping, i.e., $M_d(t) = 0.001$, $K_d(t) = 10$, $C_{d1}(t) = \text{diag}[0.1\sin([1/2]\pi t) + 0.5]$, $C_{d2}(t) = \text{diag}[0.1\sin([1/2]\pi t) + 1]$, and $C_{d3}(t) = \text{diag}[0.1\sin([1/2]\ \pi t) + 2]$. The simulation results with different magnitudes of damping are given in Fig. 7. The position of the end-effector in Cartesian space is shown in Fig. 7(a). From Fig. 7(a), it seems that the interaction performance in contact phase is not much influenced by the magnitude of damping. Besides, the zoomed-in view tracking error in noncontact phase is given in Fig. 7(b) and (c). It can be observed that, when the magnitude of damping decreases, the tracking error is reduced to improve the accuracy. The zoomed-in view velocity in contact phase is given in Fig. 7(d) and (e). It is clear that there exist some oscillations in velocity during $t \in [1.8, 2.2]$ and $t \in [5.8, 6.2]$, which is due to the change of the unknown environment, but the velocity tends to smooth immediately. From Fig. 7(d) and (e), the overshoot in the case of lowest magnitude of damping is the largest. In addition, the external force is given in Fig. 7(f), which illustrates that the external force is not much influenced by the magnitude of damping. Therefore, how to choose the magnitude of damping $C_d(t)$ depends on the specific application including the position and velocity requirements.

Case C4 (Effect of the Frequency of Damping): Consider constant inertia and stiffness, with different frequencies of damping, i.e., $M_d(t) = 0.001$, $K_d(t) = 10$, $C_{d4}(t) = \text{diag}[0.1\sin([1/2]\pi t) + 0.5]$, $C_{d5}(t) = \text{diag}[0.1\sin(5\pi t) + 0.5]$, and $C_{d6}(t) = \text{diag}[0.1\sin(15\pi t) + 0.5]$. The simulation results with different frequencies of damping are given in Fig. 8. In this case, the zoomed-in view tracking error in noncontact phase is shown in Fig. 8(b) and (c). When the frequency of damping increases, the tracking error is oscillating significantly. Fig. 8(d) and (e) plot the zoomed-in view velocity profile, which illustrates that there usually exist some oscillations when contact occurs. When the robot switches from contact phase to noncontact phase, e.g., $t \in [5.8, 6.2]$ in Fig. 8(d) and (e), the overshoot in the case of lowest frequency of damping is large obviously. Besides, from Fig. 8(f), it can be seen that the external force is not much influenced by the frequency of damping. Therefore, how to choose the frequency of damping $C_d(t)$ depends on the specific application requirements.

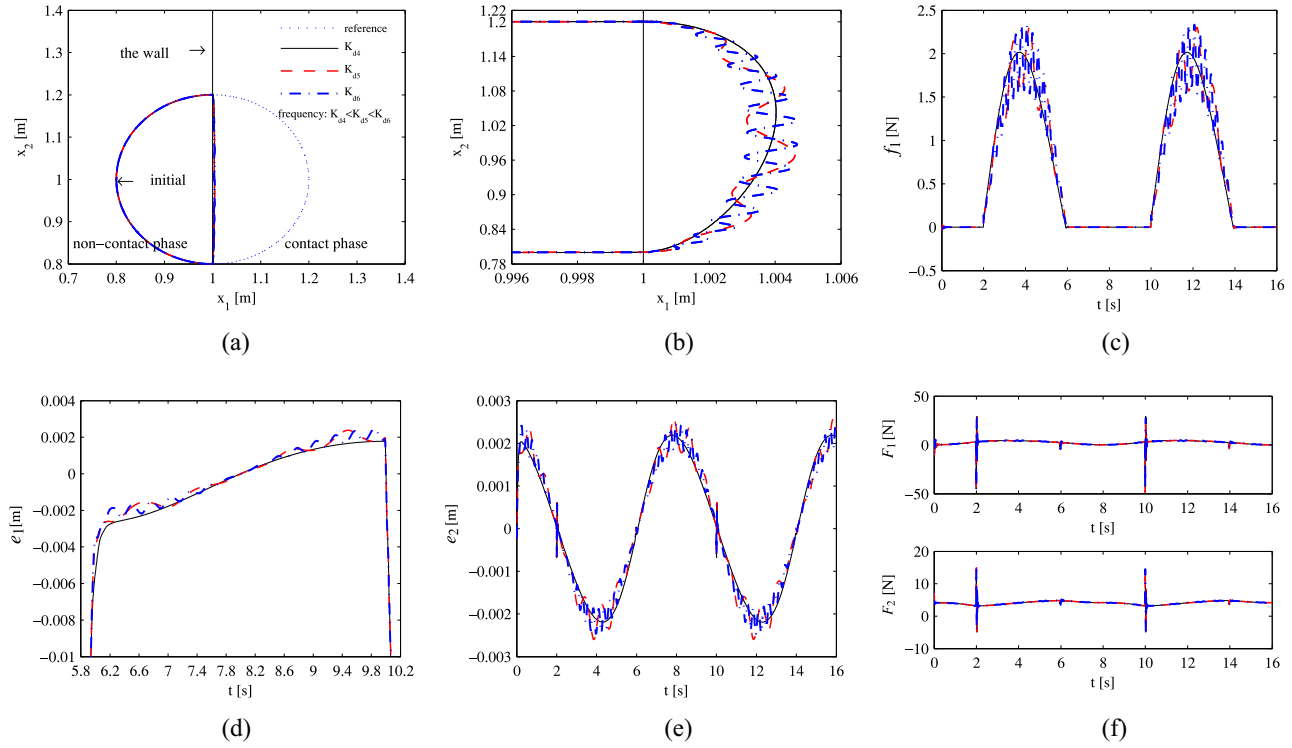

Fig. 6. Simulation results for case C2: constant inertia and damping, with different frequencies of stiffness, i.e., $M_d(t) = 0.001$, $C_d(t) = 0.5$, $K_{d4}(t) = \text{diag}[2\sin([1/2]\pi t) + 10]$, $K_{d5}(t) = \text{diag}[2\sin(5\pi t) + 10]$, and $K_{d6}(t) = \text{diag}[2\sin(15\pi t) + 10]$. (a) Positions in Cartesian space. (b) Zoomed-in view positions in contact phase. (c) External force. (d) Zoomed-in view tracking error e_1 in noncontact phase. (e) Zoomed-in view tracking error e_2 in noncontact phase. (f) Control inputs.

D. Performance With Second-Order Filters

In this section, the performance with second-order filters in the impedance control (16) will be discussed with different bandwidths presented for the purpose of comparison. A second-order filter is chosen as a Butterworth form

$$G_f(s) = \frac{1}{(T_1 s)^2 + \sqrt{2}T_1 s + 1} \tag{32}$$

where the filter parameter T_1 is tuned as 10, 0.1, and 0.001, respectively. The corresponding bandwidth is 0.1, 10, and 1000. According to the guidance of the filter design mentioned in [37], by applying the internal model principle, the information of the reference should be incorporated into the filter design. Thus, another second-order low-pass filter is chosen as follows:

$$G_f(s) = \frac{T_2 s + 2.5}{s^2 + T_2 s + 0.25\pi^2} \tag{33}$$

where the filter parameter T_2 is tuned as 0.1, 10, and 1000, respectively. The corresponding bandwidth is about 1000, 10 and 0.1. The initial position and velocity of the robot are given as $x_1(0) = [0.9\ 0.6]^T$ and $x_2(0) = [0\ 0]^T$. The desired inertia, damping, and stiffness are given by (29)–(31), with other parameters being the same as those previously defined.

The tracking error using the Butterworth filter with different bandwidths are shown in Fig. 9. From Fig. 9(a), it can be seen that when $t < 1.6$ s (i.e., in noncontact phase), the tracking error is reduced by choosing a big bandwidth. When the contact occurs at $t = 1.6$ s, the smaller bandwidth results in larger oscillation. Besides, the tracking error e_2 is shown in Fig. 9(b), and a large spike occurs in the tracking error e_2 at about $t = 1.5$ s when the bandwidth is decreased. For $2 < t < 16$ s, the three filters try to approximate the uncertain robotic dynamics. It can be observed that the big bandwidth results in the smaller and smoother tracking error.

Then, the advanced filter (33) with different bandwidths is checked and the tracking error is given in Fig. 10. It can be observed from Fig. 10(a) that when $t < 1$s, the tracking error e_1 can converge to zero faster with a bigger bandwidth. Further, the smaller bandwidth results in larger spike at about $t = 1.5$ s. Another tracking error e_2 is given in Fig. 10(b). Clearly, Fig. 10(b) implies that, if the bandwidth is selected as a small value, the oscillation occurs and the tracking error is increased.

E. Output Feedback Control Scheme

The proposed UDE-based variable impedance control (16) is designed under the assumption that all states are measurable. However, some state information may not be measurable due to practical issues such as in the absence of velocity sensors. Thus, the effectiveness of the output feedback control scheme (17) will be checked and the challenging problem of designing an output feedback control scheme using UDE is converted into the design of a low-pass filter in this section. To make sure the control structure (17) is realizable, the filter in (17) is selected as a second-order filter (32) with $T_1 = 0.001$. The desired inertia, damping and stiffness are given by (29)–(31) and other parameters are the same as previously defined in Section IV-A.

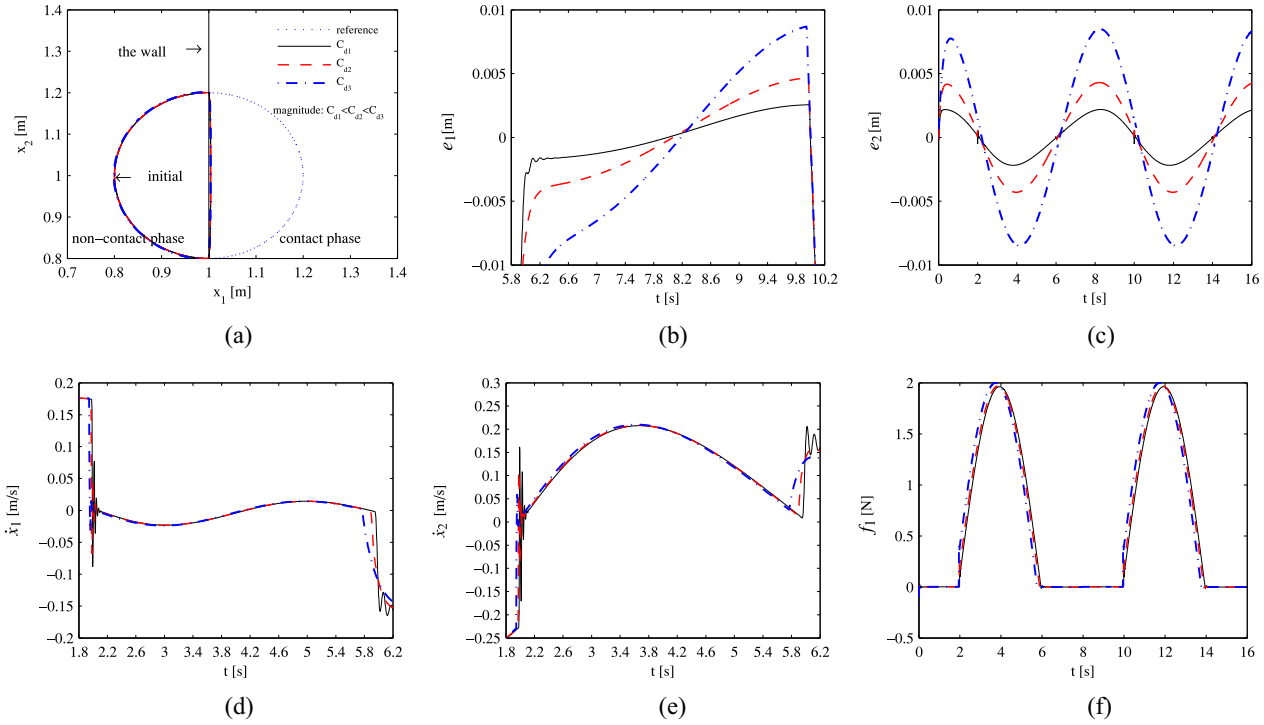

Fig. 7. Simulation results for case C3: constant inertia and stiffness, with different magnitudes of damping, i.e., $M_d(t) = 0.001$, $K_d(t) = 10$, $C_{d1}(t) = \text{diag}[0.1\sin([1/2]\pi t) + 0.5]$, $C_{d2}(t) = \text{diag}[0.1\sin([1/2]\pi t) + 1]$, and $C_{d3}(t) = \text{diag}[0.1\sin([1/2]\pi t) + 2]$. (a) Positions in Cartesian space. (b) Zoomed-in view tracking error e_1 in noncontact phase. (c) Zoomed-in view tracking error e_2 in noncontact phase. (d) Zoomed-in view velocity $\dot{x}_1$ in contact phase. (e) Zoomed-in view velocity $\dot{x}_2$ in contact phase. (f) External force.

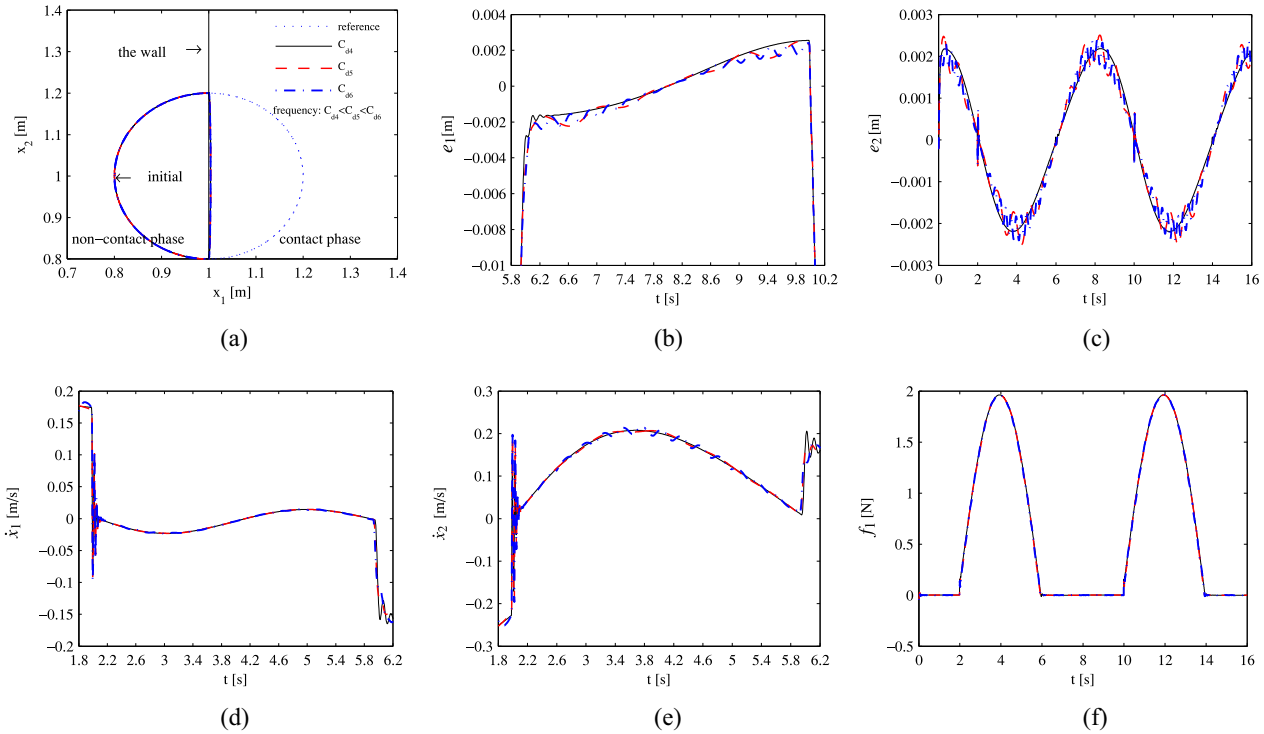

Fig. 8. Simulation results for case C4: constant inertia and stiffness, with different frequencies of damping, i.e., $M_d(t) = 0.001$, $K_d(t) = 10$, $C_{d4}(t) = \text{diag}[0.1\sin([1/2]\pi t) + 0.5]$, $C_{d5}(t) = \text{diag}[0.1\sin(5\pi t) + 0.5]$, and $C_{d6}(t) = \text{diag}[0.1\sin(15\pi t) + 0.5]$. (a) Positions in Cartesian space. (b) Zoomed-in view tracking error e_1 in noncontact phase. (c) Zoomed-in view tracking error e_2 in noncontact phase. (d) Zoomed-in view velocity $\dot{x}_1$ in contact phase. (e) Zoomed-in view velocity $\dot{x}_2$ in contact phase. (f) External force.

The simulation results using the output feedback control scheme (17) are given in Fig. 11. The position performance of x_1 is given in Fig. 11(a). Clearly, the position x_1 can track the reference in noncontact phase, and the desired destination is regulated and the end-effector slides along the wall in contact phase. The position x_2 is shown in Fig. 11(b). It is

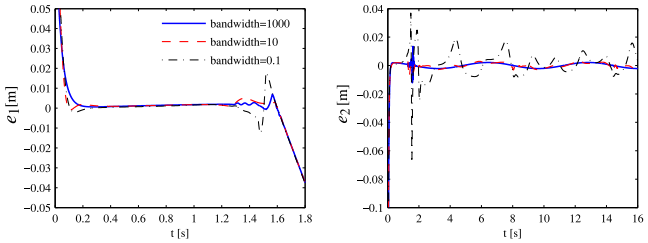

Fig. 9. Tracking errors using a Butterworth filter with different bandwidths. (a) Zoomed-in view tracking error e_1 in noncontact phase. (b) Tracking error e_2.

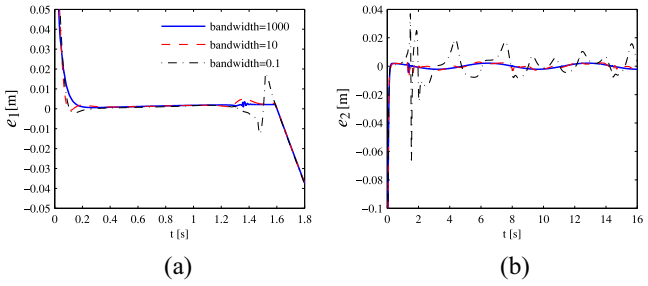

Fig. 10. Tracking errors using an advanced filter with different bandwidths. (a) Zoomed-in view tracking error e_1 in noncontact phase. (b) Tracking error e_2.

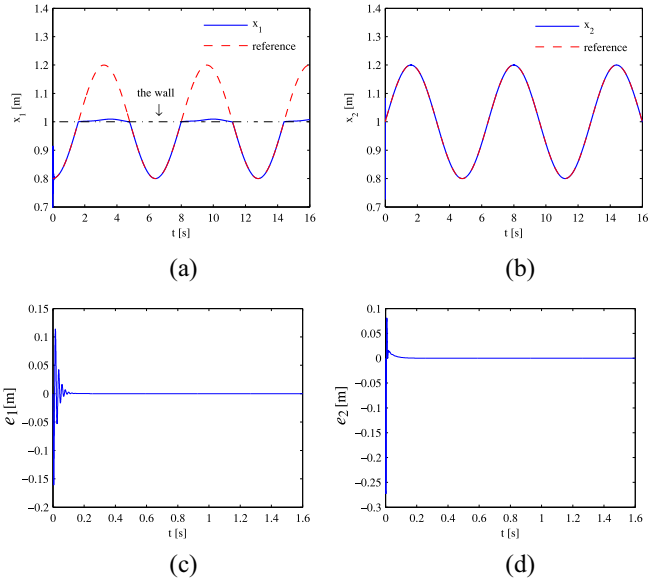

Fig. 11. Simulation results for output feedback control scheme. (a) position x_1. (b) position x_2. (c) Zoomed-in view tracking error e_1 in non-contact phase. (d) Zoomed-in view tracking error e_2 in noncontact phase.

clear that the position x_2 can track the reference trajectory in noncontact phase. Besides, the tracking errors are given in Fig. 11(c) and (d). From Fig. 11(c) and (d), it can be observed that there initially exist some oscillations for $0 < t < 0.1$, but the tracking errors can converge to small values quickly. It can be concluded that the design of an output feedback control scheme can be converted into the design of a low-pass filter.

V. Conclusion

In this paper, the UDE-based variable impedance control was developed for an uncertain robot system executing interaction tasks with its unknown environment. In particular, the variable impedance control was used to handle the change of the unknown environment. This resulted in configuration-dependent impedance dynamics. Furthermore, the UDE-based control was employed to estimate and compensate the model uncertainty. It does not require any knowledge of the uncertainty, except its bandwidth information for the control design. Extensive simulation studies showed the effectiveness of the proposed UDE-based variable impedance control in improving the robot–environment interaction performance. The guidelines for different impedance strategies were provided. Also, the proposed UDE-based variable impedance control has shown better flexibility to change the impedance dynamics during the interaction task. Besides, the performance using different filters was given to elaborate on the filter selection, and an output feedback control case was carried out to illustrate that the designing of an output feedback controller using UDE could be converted into the design of a low-pass filter, which is an improvement of the UDE-based control itself.

References

[1] V. Gandhi, G. Prasad, D. Coyle, L. Behera, and T. M. McGinnity, "EEG-based mobile robot control through an adaptive brain–robot interface," *IEEE Trans. Syst., Man, Cybern., Syst.*, vol. 44, no. 9, pp. 1278–1285, Sep. 2014.

[2] Z. Liu, C. Chen, Y. Zhang, and C. L. P. Chen, "Adaptive neural control for dual-arm coordination of humanoid robot with unknown nonlinearities in output mechanism," *IEEE Trans. Cybern.*, vol. 45, no. 3, pp. 507–518, Mar. 2015.

[3] M. Li, Y. Li, S. S. Ge, and T. H. Lee, "Adaptive control of robotic manipulators with unified motion constraints," *IEEE Trans. Syst., Man, Cybern., Syst.*, vol. 47, no. 1, pp. 184–194, Jan. 2017.

[4] W. He and S. Zhang, "Control design for nonlinear flexible wings of a robotic aircraft," *IEEE Trans. Control Syst. Technol.*, vol. 25, no. 1, pp. 351–357, Jan. 2017.

[5] N. Hogan, "Impedance control—An approach to manipulation. I—Theory. II—Implementation. III—Applications," *Trans. J. Dyn. Syst. Meas. Control ASME*, vol. 107, pp. 1–24, Mar. 1985.

[6] S. Jung, T. C. Hsia, and R. G. Bonitz, "Force tracking impedance control of robot manipulators under unknown environment," *IEEE Trans. Control Syst. Technol.*, vol. 12, no. 3, pp. 474–483, May 2004.

[7] S. Yi, "Stable walking of qauadruped robot by impedance control for body motion," *Int. J. Control Autom.*, vol. 6, no. 2, pp. 99–110, 2013.

[8] Y. Sano, R. Hori, and T. Yabuta, "Comparison between admittance and impedance control method of a finger-arm robot during grasping object with internal and external impedance control," *Nihon Kikai Gakkai Ronbunshu C Hen/Trans. Japan Soc. Mech. Eng. C*, vol. 79, no. 807, pp. 4330–4334, 2013.

[9] W. He and Y. Dong, "Adaptive fuzzy neural network control for a constrained robot using impedance learning," *IEEE Trans. Neural Netw. Learn. Syst.*, to be published, doi: 10.1109/TNNLS.2017.2665581.

[10] H. Mehdi and O. Boubaker, "Stiffness and impedance control using Lyapunov theory for robot-aided rehabilitation," *Int. J. Soc. Robot.*, vol. 4, no. 1, pp. 107–119, Nov. 2012.

[11] S. Hussain, S. Q. Xie, and P. K. Jamwal, "Adaptive impedance control of a robotic orthosis for gait rehabilitation," *IEEE Trans. Cybern.*, vol. 43, no. 3, pp. 1025–1034, Jun. 2013.

[12] L. Huang, S. S. Ge, and T. H. Lee, "Fuzzy unidirectional force control of constrained robotic manipulators," *Fuzzy Sets Syst.*, vol. 134, no. 1, pp. 135–146, 2003.

[13] Y. Li, S. S. Ge, and C. Yang, "Learning impedance control for physical robot–environment interaction," *Int. J. Control*, vol. 85, no. 2, pp. 182–193, 2012.

[14] Z. Li *et al.*, "Decentralized fuzzy control of multiple cooperating robotic manipulators with impedance interaction," *IEEE Trans. Fuzzy Syst.*, vol. 23, no. 4, pp. 1044–1056, Aug. 2015.
[15] S. Suzuki and K. Furuta, "Adaptive impedance control to enhance human skill on a haptic interface system," *J. Control Sci. Eng.*, vol. 2012, pp. 1–10, Jan. 2012.
[16] Y. Li and S. S. Ge, "Human–robot collaboration based on motion intention estimation," *IEEE/ASME Trans. Mechatronics*, vol. 19, no. 3, pp. 1007–1014, Jun. 2014.
[17] H. Modares, I. Ranatunga, F. L. Lewis, and D. O. Popa, "Optimized assistive human–robot interaction using reinforcement learning," *IEEE Trans. Cybern.*, vol. 46, no. 3, pp. 655–667, Mar. 2016.
[18] M. R. Williams, S. D'Andrea, and H. M. Herr, "Impact on gait biomechanics of using an active variable impedance prosthetic knee," *J. Neuroeng. Rehabil.*, vol. 13, no. 1, p. 54, 2016.
[19] E. Burdet, R. Osu, D. W. Franklin, T. E. Milner, and M. Kawato, "The central nervous system stabilizes unstable dynamics by learning optimal impedance," *Nature*, vol. 414, no. 6862, pp. 446–449, 2001.
[20] L. P. J. Selen, D. W. Franklin, and D. M. Wolpert, "Impedance control reduces instability that arises from motor noise," *J. Neurosci. Official J. Soc. Neurosci.*, vol. 29, no. 40, pp. 12606–12616, 2009.
[21] C. Ott, *Cartesian Impedance Control of Redundant and Flexible-Joint Robots*, vol. 49. New York, NY, USA: Springer, 2008.
[22] F. Ferraguti, C. Secchi, and C. Fantuzzi, "A tank-based approach to impedance control with variable stiffness," in *Proc. IEEE Conf. Robot. Autom.*, Karlsruhe, Germany, 2013, pp. 4948–4953.
[23] F. Ficuciello, L. Villani, and B. Siciliano, "Variable impedance control of redundant manipulators for intuitive human–robot physical interaction," *IEEE Trans. Robot.*, vol. 31, no. 4, pp. 850–863, Aug. 2015.
[24] B. Vanderborght *et al.*, "Variable impedance actuators: A review," *Robot. Auton. Syst.*, vol. 61, no. 12, pp. 1601–1614, 2013.
[25] K. Kronander and A. Billard, "Stability considerations for variable impedance control," *IEEE Trans. Robot.*, vol. 32, no. 5, pp. 1298–1305, Oct. 2016.
[26] D. K. Das, S. Ghosh, and B. Subudhi, "An improved robust stability analysis for systems with two delays by extracting overlapping feature," *J. Control Decis.*, vol. 2, no. 2, pp. 124–141, 2015.
[27] W. He and S. S. Ge, "Cooperative control of a nonuniform gantry crane with constrained tension," *Automatica*, vol. 66, pp. 146–154, Apr. 2016.
[28] W. He, Y. Ouyang, and J. Hong, "Vibration control of a flexible robotic manipulator in the presence of input deadzone," *IEEE Trans. Ind. Informat.*, vol. 13, no. 1, pp. 48–59, Feb. 2017.
[29] Y. Pan and G.-H. Yang, "Event-triggered fuzzy control for nonlinear networked control systems," *Fuzzy Sets Syst.*, vol. 329, pp. 91–107, Dec. 2017.
[30] Y. Pan and G.-H. Yang, "Event-triggered fault detection filter design for nonlinear networked systems," *IEEE Trans. Syst., Man, Cybern., Syst.*, to be published, doi: 10.1109/TSMC.2017.2719629.
[31] M. M. Bridges, D. M. Dawson, and C. T. Abdallah, "Control of rigid-link, flexible-joint robots: A survey of backstepping approaches," *J. Robot. Syst.*, vol. 12, no. 3, pp. 199–216, 1995.
[32] S. J. Yoo, J. B. Park, and Y. H. Choi, "Adaptive dynamic surface control of flexible-joint robots using self-recurrent wavelet neural networks," *IEEE Trans. Syst., Man, Cybern. B, Cybern.*, vol. 36, no. 6, pp. 1342–1355, Dec. 2006.
[33] S. J. Yoo, J. B. Park, and Y. H. Choi, "Adaptive output feedback control of flexible-joint robots using neural networks: Dynamic surface design approach," *IEEE Trans. Neural Netw.*, vol. 19, no. 10, pp. 1712–1726, Oct. 2008.
[34] Q.-C. Zhong and D. Rees, "Control of uncertain LTI systems based on an uncertainty and disturbance estimator," *ASME Trans. J. Dyn. Syst. Meas. Control*, vol. 126, no. 4, pp. 905–910, Dec. 2004.
[35] R. K. Stobart, A. Kuperman, and Q.-C. Zhong, "Uncertainty and disturbance estimator–based control for uncertain LTI-SISO systems with state delays," *ASME Trans. J. Dyn. Syst. Meas. Control*, vol. 133, no. 2, pp. 1–6, 2011.
[36] B. Ren, Q.-C. Zhong, and J. Chen, "Robust control for a class of nonaffine nonlinear systems based on the uncertainty and disturbance estimator," *IEEE Trans. Ind. Electron.*, vol. 62, no. 9, pp. 5881–5888, Sep. 2015.
[37] B. Ren, Q.-C. Zhong, and J. Dai, "Asymptotic reference tracking and disturbance rejection of UDE-based robust control," *IEEE Trans. Ind. Electron.*, vol. 64, no. 4, pp. 3166–3176, Apr. 2017.
[38] T. Chandrasekhar and L. Dewan, "Sliding mode control based on TDC and UDE," *Int. J. Informat. Syst. Sci.*, vol. 3, no. 1, pp. 36–53, 2007.
[39] P. Shendge and B. Patre, "Robust model following load frequency sliding mode controller based on UDE and error improvement with higher order filter," *IAENG Int. J. Appl. Math.*, vol. 37, no. 1, pp. 27–32, 2007.
[40] Y. Wang, B. Ren, and Q.-C. Zhong, "Robust power flow control of grid-connected inverters," *IEEE Trans. Ind. Electron.*, vol. 63, no. 11, pp. 6887–6897, Nov. 2016.
[41] S. Su and Y. Lin, "Robust output tracking control for a velocity-sensorless vertical take-off and landing aircraft with input disturbances and unmatched uncertainties," *Int. J. Robust Nonlin. Control*, vol. 23, pp. 1198–1213, Jul. 2013.
[42] B. Ren, Y. Wang, and Q.-C. Zhong, "UDE-based control of variable-speed wind turbine systems," *Int. J. Control*, vol. 90, no. 1, pp. 121–136, Jan. 2017.
[43] J. Chen, B. Ren, and Q.-C. Zhong, "UDE-based trajectory tracking control of piezoelectric stages," *IEEE Trans. Ind. Electron.*, vol. 63, no. 10, pp. 6450–6459, Oct. 2016.
[44] J. P. Kolhe, M. Shaheed, T. S. Chandar, and S. E. Taloe, "Robust control of robot manipulators based on uncertainty and disturbance estimation," *Int. J. Robust Nonlin. Control*, vol. 23, no. 1, pp. 104–122, Jan. 2013.
[45] S. S. Ge, T. H. Lee, and C. J. Harris, *Adaptive Neural Network Control of Robotic Manipulators*. London, U.K.: World Sci., 1998.
[46] W. He, Y. Chen, and Z. Yin, "Adaptive neural network control of an uncertain robot with full-state constraints," *IEEE Trans. Cybern.*, vol. 46, no. 3, pp. 620–629, Mar. 2016.
[47] J. C. Willems, "Dissipative dynamical systems part I: General theory," *Archive Ration. Mech. Anal.*, vol. 45, no. 5, pp. 321–351, 1972.
[48] Q.-C. Zhong, A. Kuperman, and R. Stobart, "Design of UDE-based controllers from their two-degree-of-freedom nature," *Int. J. Robust Nonlin. Control*, vol. 21, no. 17, pp. 1994–2008, Nov. 2011.
[49] W. He, Y. Dong, and C. Sun, "Adaptive neural impedance control of a robotic manipulator with input saturation," *IEEE Trans. Syst., Man, Cybern., Syst.*, vol. 46, no. 3, pp. 334–344, Mar. 2016.
[50] N. Hogan and S. P. Buerger, "Impedance and interaction control," in *Robotics and Automation Handbook*, vol. 1. Boca Raton, FL, USA: CRC Press, 2005.

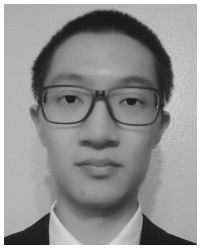

Yiting Dong (S'14) received the B.Eng. degree from the School of Automation Engineering, University of Electronic Science and Technology of China (UESTC), Chengdu, China, in 2014 and the M.Eng. degree in control science and engineering from UESTC, in 2017. He is currently pursuing the Ph.D. degree in the Department of Mechanical Engineering, Texas Tech University, Lubbock, TX, USA.

His current research interests include robust control, robotic control, and power electronics control.

Beibei Ren (S'05–M'10) received the B.Eng. degree in the mechanical and electronic engineering and the M.Eng. degree in automation from Xidian University, Xi'an, China, in 2001 and in 2004, respectively, and the Ph.D. degree in electrical and computer engineering from the National University of Singapore, Singapore, in 2010.

From 2010 to 2013, she was a Post-Doctoral Scholar in the Department of Mechanical and Aerospace Engineering, University of California at San Diego, San Diego, CA, USA. Since 2013, she has been with the Department of Mechanical Engineering, Texas Tech University, Lubbock, TX, USA, as an Assistant Professor. Her current research interests include robust control, power electronics control, renewable energy, microgrid, and navigation and control of autonomous vehicles.